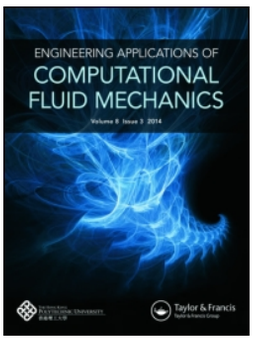

Engineering Applications of Computational Fluid Mechanics

ISSN: 1994-2060 (Print) 1997-003X (Online) Journal homepage: http://www.tandfonline.com/loi/tcfm20

Numerical study of the aerodynamics of sound sources in a bass-reflex port

V.M. Garcia-Alcaide, S. Palleja-Cabre, R. Castilla, P. J. Gamez-Montero, J. Romeu, T. Pamies, J. Amate & N. Milan

To cite this article: V.M. Garcia-Alcaide, S. Palleja-Cabre, R. Castilla, P. J. Gamez-Montero, J. Romeu, T. Pamies, J. Amate & N. Milan (2017) Numerical study of the aerodynamics of sound sources in a bass-reflex port, Engineering Applications of Computational Fluid Mechanics, 11:1, 210-224, DOI: 10.1080/19942060.2016.1277166

To link to this article: http://dx.doi.org/10.1080/19942060.2016.1277166

ENGINEERING APPLICATIONS OF COMPUTATIONAL FLUID MECHANICS, 2017
VOL. 11, NO. 1, 210–224
http://dx.doi.org/10.1080/19942060.2016.1277166

Taylor & Francis
Taylor & Francis Group

Numerical study of the aerodynamics of sound sources in a bass-reflex port

V. M. Garcia-Alcaide[a], S. Palleja-Cabre[a], R. Castilla [a], P. J. Gamez-Montero [a], J. Romeu [a], T. Pamies [b], J. Amate[c] and N. Milan[c]

[a]LABSON, Department of Fluid Mechanics, Universitat Politècnica de Catalunya, Spain; [b]LEAM, Department of Mechanical Engineering, Universitat Politècnica de Catalunya, Spain; [c]AMATE AUDIO S.L., Terrassa, Spain

ABSTRACT

The aim of this paper is to study the aerodynamics phenomena of a bass-reflex port that causes noise in the audible frequency range. After discarding structural and mechanical vibration issues, the hypothesis considered is that vortex shedding is the source of the noise. Experimental and numerical evidences of the vortex, an analysis of its noise and the similarities between real and simulated performance are presented. The numerically simulated cases with the original geometry are excited at different frequencies and with modifications of the port geometry. Likewise, the internal performance of an enclosure with a closed port was simulated. The simulations have been performed with axisymmetrical geometries using the open-source OpenFOAM® toolbox. Moreover, experimental measurements were carried out. First, acoustic signal experiments were done to analyse the response of the bass-reflex ports. Secondly, a structure vibration measurement was conducted in order to exclude the cabinet structure vibration as a source of the noise in question. A good agreement was found between numerical and experimental results, especially in the frequency band of the detected noise, i.e. the 1000–1500 Hz range. Despite no remarkable improvement being made with the geometry changes explored, the presented CFD approach has proved a useful and cost-effective tool to address this kind of phenomenon.

ARTICLE HISTORY
Received 26 April 2016
Accepted 23 December 2016

KEYWORDS
Bass reflex port; vortex shedding; Helmholtz resonance frequency; aerodynamic noise; dynamic mesh

Nomenclature

A	Velocity gradient tensor
c	Velocity of sound
c_p	Specific heat at constant pressure for air
ψ	Compressibility
$\vec{U}$	Advection velocity in boundary
D	Woofer diameter
f	Frequency
L_{Eff}	Effective length of bass-reflex port
μ	Viscosity of air
p	Air pressure
Q	Second invariant of velocity gradient tensor
$\mathbb{R}$	Gas constant for air
ρ	Air density
R	Radius of bass-reflex port
St_R	Strouhal number based on length R
r	End rounding of port
S_0	Area of bass-reflex port
k	Air thermal conductivity
T	Air temperature
u	Flow velocity
V	Internal volume of loudspeaker box
X_{max}	Maximum amplitude of woofer
ω	Angular frequency ($2\pi f$)

1. Introduction

A bass-reflex enclosure is a sealed box in which a port has been placed. This bass-reflex port connects the interior volume of air with the exterior. The enclosure becomes similar to a Helmholtz resonator and its gains are higher at frequencies near the Helmholtz frequency (see Equation 1) (Roozen, Bockholts, Eck, & Hirschberg, 1998b). In the usual boxes it takes low-frequency values, and that is why the enclosure is used to improve low-frequency performance.

However, bass-reflex loudspeakers can cause an uncomfortable blowing noise when excited at certain frequencies because of the vortices generated due to the air velocity on the exhaust flow.

With regard to this phenomenon, researchers at Philips Research Laboratories and Eindhoven University of Technology found that vortices are generated at both ends of the port of the bass reflex during each cycle (Roozen et al., 1998b). A vortex shedding takes place

CONTACT R. Castilla castilla@mf.upc.edu

at the transitional area where the air flows out of the port into the ambient air, and also into the port, when a sharp-edged port termination is used. There, mushroom-shaped vortices are generated each time the air flows out of the port. These vortices produce acoustic waves in the longitudinal direction of the port in an impulsive manner.

To measure the vortices, researchers at the Department of Mechanics of the Università Politecnica delle Marche have carried out a pioneering study (Rossi, Esposito, & Tomasini, 2008). In their work the authors used Laser Doppler Anemometry (LDA) and Particle Image Velocimetry (PIV) methods to measure such flows in bass-reflex systems under operating conditions. In particular, due to the whole field nature of PIV, researchers were able to locate the presence of vortices and flow instabilities. In addition, by using LDA the velocity behaviour over time and its dispersion in a particular point could be determined for different input power.

Some solutions for reducing the blowing noise include, on one hand, a gradual widening of the port toward both port ends to obtain a converging–diverging port cross section (Roozen et al., 1998b). With the widening and the increase of area at the port ends, the local air velocity is reduced and it is less likely that vortices will be generated, or they will be less intense. On the other hand, rounding the edges at both ends of the port can eliminate the vortex shedding at the inlet side of the port and can considerably reduce the vortex shedding at the port's outlet side, as long as the Strouhal number is greater than one.

The Strouhal number (Equation 2) is a dimensionless quantity based on the radius of the edge's curvature which determines flow separation in the case of unsteady flows. It is reported to be an objective indicator of ability to suppress blowing sounds at the point of separation (Roozen et al., 1998b; Salvatti, Devantier, & Button, 2002) because it seems to predict the beginning of severe vortex shedding.

Even though several studies of a bass-reflex enclosure had been done (Backman, 1995, 2012; Rapoport & Devantier, 2004; Roozen, Bockholts, Eck, & Hirschberg, 1998a; Roozen et al., 1998b; Roozen, Vael, & Nieuwendijk, 1998; Salvatti et al., 2002; Vanderkooy, 1998), few of them include CFD simulations and a wide range of different experimental tests. As far as the authors know, only in Rapoport & Devantier (2004) are turbulent simulations performed with several ports designed and top performance sought.

According to Roozen et al. (1998b), a flared ending port would appreciably reduce the generated vortex and, presumably, the midrange noise. Nevertheless, it would imply more complicated and expensive manufacturing.

In the present study, the performance of a loudspeaker bass-reflex port is characterised numerically – in particular, one that produces a blowing noise – and the results compared with experimental measurement. The problem has been addressed numerically by using OpenFOAM® and experimentally through several experiments with open and closed ports, considering the hypothesis that vortex shedding could be the source of the noise. The air movement has been simulated with a dynamic mesh in the driver wall. This performs a better simulation of the flow entrance in a bass-reflex port, since it not only prescribes the velocity, but also the pressure and density, which would be difficult to define with the usual definition of inlet boundary conditions. To the best knowledge of the authors there is no publication on the CFD simulation of a bass reflex with this method.

The purpose of the present work is to provide a numerical and affordable tool for the design and simulation of bass-reflex ports including vortex shedding and its effects in terms of noise level. Improving port geometry is beyond the scope of the present work.

2. Methodology

2.1. Problem statement

The actual geometry studied, depicted in Figure 1, has two identical bass-reflex ports. The geometrical data of the port and the loudspeaker, as well as the main woofer specifications, are shown in Table 1. Figure 2 displays the loudspeaker frequency response, as measured in the laboratory. The bass-reflex ports act as Helmholtz resonators with a frequency of 50 Hz, according to Equation (1):

$$f_{\text{Helmholtz}} = \frac{c}{2\pi}\sqrt{\frac{S_0}{L_{\text{Eff}}V}}. \tag{1}$$

This bass-reflex port geometry has been proven to generate a blowing noise when the loudspeaker is excited near the Helmholtz resonance frequency. This noise seems to dissipate when bass-reflex ports are closed. That suggests that this noise is related to the exhaust flow in the port, since the value of the Strouhal number, given by

$$\text{St}_R = \frac{\omega r}{u} \tag{2}$$

is, in our case, less than 0.2. According to Roozen et al. (1998a) and Salvatti et al. (2002), this means pronounced vortex shedding.

2.2. Experimental measurements

The objective of the experimental approach was to determine the performance of the device to compare it with

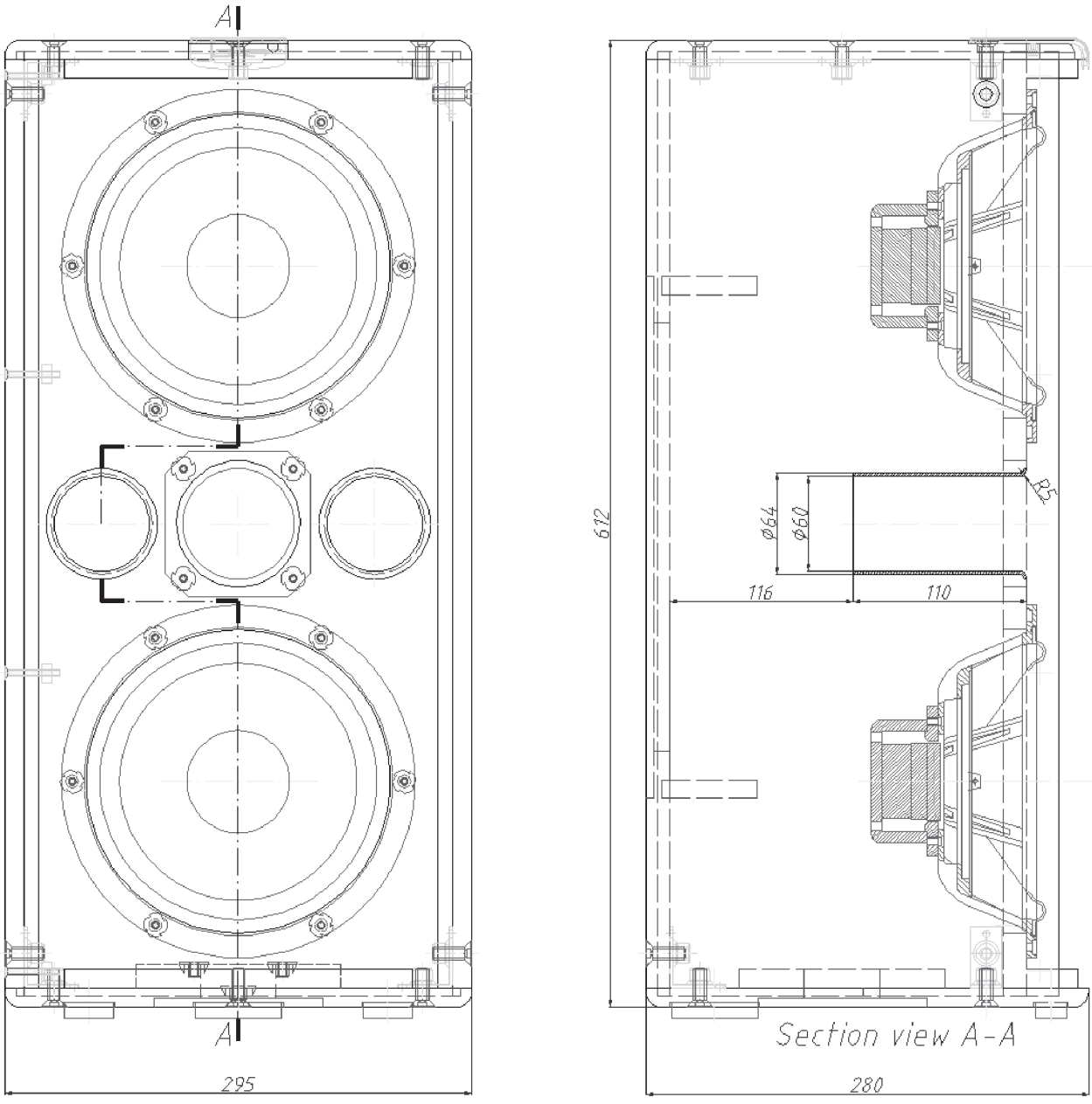

Figure 1. The analysed loudspeaker with bass reflex geometry. All dimensions are in millimetres.

Table 1. Main features of the loudspeaker and bass-reflex ports.

Feature	Value
R	30 *mm*
L_{Eff}	110 *mm*
r	5 *mm*
V	30.50×10^{-3} m^3
D	150 *mm*
X_{max}	± 4.5 *mm*
Sensitivity at 1 W/m	90.8 dB SPL
Impedance	8 Ω

Note: SPL, Sound Pressure Level.

CFD results. First of all, a set of acoustic measurements was carried out with the loudspeaker driven by harmonic signals of 40, 50, 65 and 80 Hz in a semi-anechoic chamber.

To ensure that the noise has aerodynamic origins and to discard structural vibrations as the noise source, a mechanical vibration experiment was performed as well. Finally, the exhaust flow was visualised with smoke and a high-speed camera.

2.2.1. Acoustic measurements

The sound was produced with an NTI AG Minirator MR1 audio generator, which generates 31 pure sinusoidal signals in intervals of one third of an octave steps. Three different signal amplitudes, -4, 0 and $+4$ *dBV*, were used for signal excitation. This signal was amplified so that the loudspeaker received $+22$, $+26$ and $+30$ *dBV*

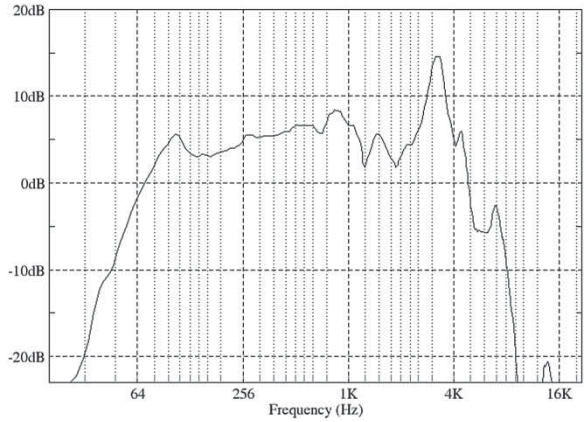

Figure 2. Frequency response of loudspeaker.

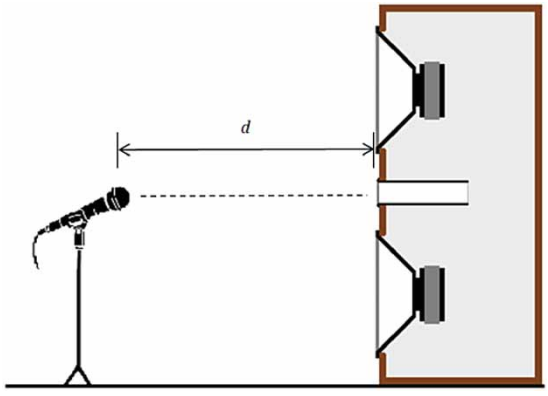

Figure 3. Scheme for acoustic measurement with a GRASS 40 AE microphone. $d = 200$ mm.

excitation levels. The sensitivity of the loudspeaker is listed in Table 1, and the response to the excitation frequencies is plotted in Figure 2. The sound emitted by the loudspeaker was captured by a GRASS 40 AE microphone at a distance of 200 mm and aligned with the ports connected to an LMS Pimento signal analyser in a semi-anechoic chamber (see Figure 3). The microphone was equipped with a windscreen in order to avoid the potential effect of air flow coming from the port. Then it was post-processed in order to obtain the frequency spectrum of the generated sound. The experiments were done with the enclosure open and closed to see the effect of the bass reflex on the device's performance.

Although the 0.2 m distance is small compared with the wavelength associated with low-frequency sound, it is considered appropriated for sound recording in the medium range, between 1000 and 1500 Hz, of interest in the present work.

2.2.2. Mechanical vibration measurements

To ensure that the noise has an aerodynamic and not structural origin, triaxial vibration measurements were carried out at different points of the loudspeaker. The vibration was captured with a PIOTRONIC ADXL335 three-axis acceleration sensor connected to an LMS Pimento signal analyser. The accelerometer position is depicted in Figure 4. The signals were processed and stored. As in the previous experiment, both open and closed cases were considered.

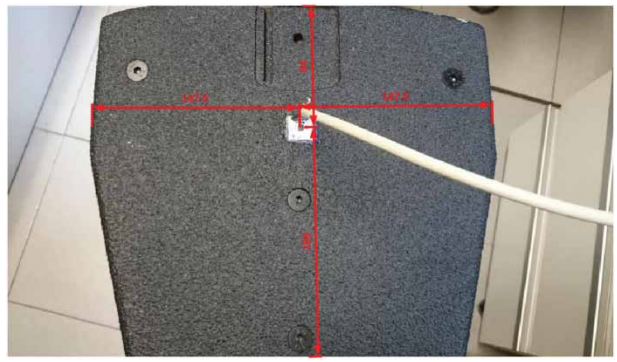

Figure 4. Position of the PIOTRONIC ADXL335 accelerometer in the top side of the loudspeaker for mechanical vibration measurements. Distances are in millimetres.

2.2.3. Flow visualisation

The port generated vortex was captured with a Photron Ultima FASTCAM APX-RS high-speed camera with a recording frequency of 3000 fps. The inside of the enclosure was seeded with 1.5 μm of Shell Ondina Oil 15, produced with a Teknova RG100 fog generator. The flow was illuminated with an IR laser, which was synchronised with the camera with a TTi TG2000 function generator. The domain of interrogation was in front of the bass-reflex port and its dimensions were 190 × 190 mm.

2.3. Numerical approach

For the numerical approach of the case, an axisymmetrical approximation was carried out. This approximation has proven to resemble reality while simplifying the equations and reducing the required computational power (Rapoport & Devantier, 2004). Three-dimensional simulations were also explored, but the time consumption proved to be much larger (about 700 times larger than 2D axisymmetrical simulations) and the velocity field was similar in our interest zone, in the exit of the bass-reflex port (see Figure 5). Therefore, the 2D axisymmetrical approach was adopted.

A single port identical to the original was simulated, but given that the box has two ports, the enclosure is only half of the original volume. This fact increases the Helmholtz frequency, by a factor $\sqrt{2}$, with respect to the original box from 50 to 71 Hz, if the ports are assumed to work independently. The simulations were performed

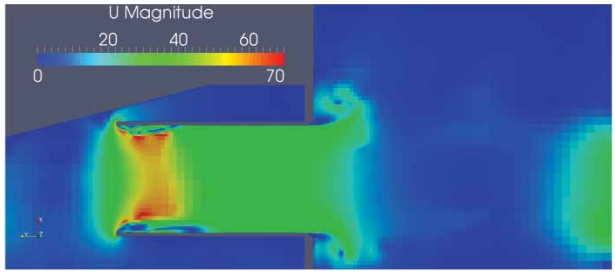

Figure 5. U field for 3D simulation for a 65 Hz excitation and $t \approx 7T/8$.

at a frequency of 65 Hz, since that is the closest to the bass-reflex resonance frequency among the available frequencies in the experiments.

The following are the additional points to consider.

- The port geometry must be totally conserved. The port is a cylinder with a rounding of 5 mm on the outlet, therefore its axis will be the symmetry axis. The port radius is 30 mm and its length is 110 mm.
- The distance between the port and the rear wall is also conserved. The rear wall is 116 mm away from the internal port end (see Figure 1)
- The volume per port is considered to be the same as the real enclosure, i.e. half the value of the volume given in Table 1. Considering that this volume must be distributed into an axisymmetric space with a known length along the axis (226 mm), the radius of the simulated enclosure has to be 146.6 mm in order to preserve the enclosure volume.
- The original geometry has two speakers. Given that only one port and half of the volume is simulated, only one speaker will be simulated. The speaker cannot be placed in its original place in an axisymmetrical configuration, and likewise cannot be placed on the axis of the geometry maintaining its original circular-like shape. Therefore the speaker will be simulated with an annular shape. The mean radius of the annulus will be at $r_m = 82$ mm from the centre. The actual woofer surface is $A = 17.67 \times 10^{-3}\ m^2$, and the distance x between the mean radius and the exterior or interior radius can be calculated as $A = \pi\left[(r_m + x)^2 - (r_m - x)^2\right] \Rightarrow x = 17$ mm. See Figure 6.
- The exterior must be big enough to capture the vortex at the outlet of the port. A cylinder with a radius of 200 mm and a length of 400 mm from the port end to outside has performed well without increasing the computation time.

The blocks used to mesh and the positions of the probes, represented as red dots, can be seen in Figure 7. The domain is meshed with 66,612 hexahedrals and

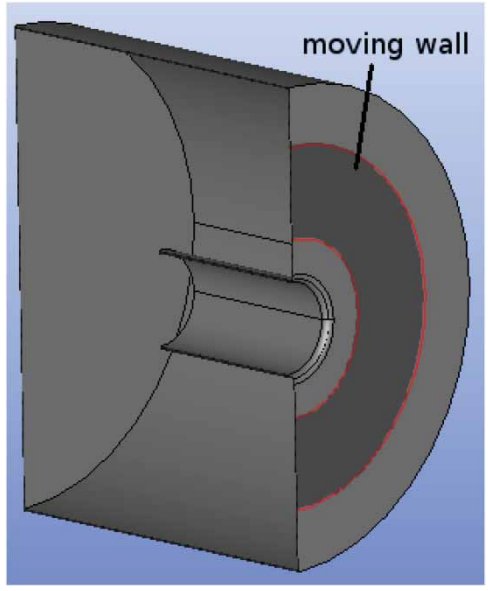

Figure 6. Three-dimensional scheme for the numerical model. The annular model of the driver is marked in red.

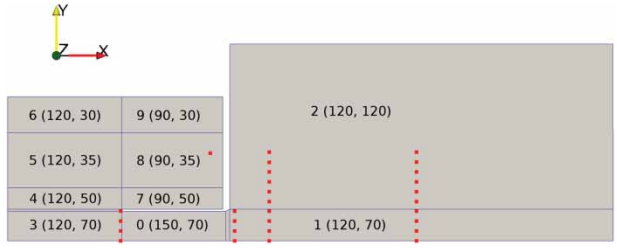

Figure 7. Blocks and probes used. The first number on each block is its numeration. The numbers in brackets are the divisions that have been made to build the mesh on the *x*- and *y*-axes, respectively. On the *z*-axis, only one cell is used due to axisymmetry. The enclosure comprises blocks 3 to 7. The bass-reflex port is block 0.

398 prisms, where the latter are located over the axis of axisymmetry. It must be noted that the box is placed on the left side of the figure (blocks 3 to 9), the axis of the axisymmetry is parallel to x and placed on the bottom and the exterior are on the right side (blocks 1 and 2). All blocks except the port (block 0) feature a small gradient to capture the flow at the port's end. In order to sample fields in the exterior space, the probe located over the axis and farthest of the port (at 0.2 m) will be analysed. According to Middelberg, Barber, Leong, Byrne, & Leonardi (2004), this mesh fulfils the requirements of accuracy in terms of time step, which is 10 μ s. It is less than the Nyquist frequency (50 kHz) and the maximum mesh size, about 3 mm, is smaller than the Nyquist wavelength.

The driver is approximated as a moving piston with an oscillation amplitude of 4.5 mm, which is the X_{max} parameter in Table 1, with an annular shape. This movement only affects the inside of the enclosure. The

movement of the driver is simulated with a moving wall in a dynamic mesh. The cells close to the driver are deformed with the wall motion, so that the velocity and pressure are transmitted inside the loudspeaker case. Note that outside the enclosure there is only the perturbation that radiates through the port.

The solver used was `rhoPimpleDyMFoam`, which is included in OpenFOAM®, an open-source Computational Fluid Dynamics toolbox (Weller, Tabor, Jasak, & Fureb, 1998). It solves the transient and compressible flow dynamics equations

$$\frac{\partial \rho}{\partial t} + \nabla \cdot \left(\rho \vec{u}\right) = 0 \tag{3}$$

$$\frac{\partial}{\partial t}\left(\rho \vec{u}\right) + \nabla \cdot \left(\rho \vec{u}\vec{u}\right) = -\nabla p + \nabla \cdot \left\{\mu \left[\nabla \vec{u} + \left(\nabla \vec{u}\right)^{\mathrm{T}}\right]\right\} - \frac{2}{3}\nabla\left(\mu \nabla \cdot \vec{u}\right) \tag{4}$$

along with an equation for energy

$$\frac{\partial}{\partial t}\left(\rho c_p T\right) + \nabla \cdot \left(\rho c_p T \vec{u}\right) = \nabla \cdot \left(k \nabla T\right) + \frac{\mathrm{D}p}{\mathrm{D}t} - \frac{2}{3}\mu\left(\nabla \cdot \vec{u}\right)^2 \tag{5}$$

and an equation of state, which for an ideal gas is given by

$$\rho = \frac{p}{\mathbb{R}T}, \tag{6}$$

where $\mathbb{R}$ is the gas constant. These equations are solved with a Finite Volume Method (FVM) featuring a dynamic mesh and PIMPLE algorithm. PIMPLE is a combination of SIMPLE (Semi-Implicit Method for Pressure-Linked Equations) and PISO (Pressure Implicit with Splitting of Operators). The flow chart of the PIMPLE algorithm over a time step can be seen in Figure 8. For the transient term, a implicit first-order Euler scheme is used. The CFL number was limited to one in order to guarantee numerical stability. The divergence scheme is a second-order linear upwind scheme (Greenshields, 2015).

Ideally, the outlet boundary should transmit the acoustic pressure without any reflection (Torregrosa, Fajardo, Gil, & Navarro, 2012). Although there is no implementation of a boundary condition in the OpenFOAM® distribution that can completely avoid wave reflections, in the present simulations the `waveTransmissive` boundary condition was used in the pressure field in order to minimise these sound wave reflections (Poinsot & Lelef, 1992). This boundary condition solves the advection equation for the compressibility

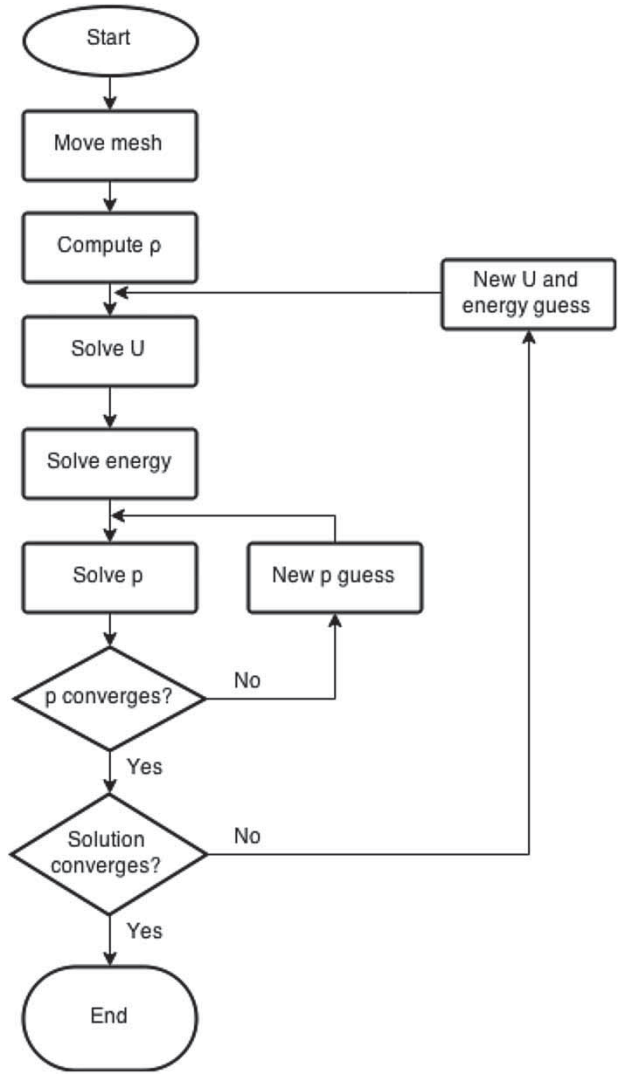

Figure 8. PIMPLE algorithm flowchart.

field:

$$\frac{\partial \psi}{\partial t} + \nabla \cdot \left(\psi \vec{U}\right) = 0 \tag{7}$$

where $\psi = \left(\partial p / \partial \rho\right)_T$ is the compressibility field and $\vec{U} = \vec{u} + \sqrt{\gamma/\psi}$ is the advection velocity. Nevertheless, this boundary condition cannot avoid a small fraction of the wave being reflected (Schmalz & Kowalczyk, 2015).

The dynamic mesh feature is used in the woofer simulation (see Figure 6), where the moving wall pushes the fluid domain with a prescribed movement. The time scheme followed was the Euler method. The Laplacians, divergences, gradients and interpolations have been modelled with linear approximations, except for the divergence of the velocity, turbulence kinetic energy and enthalpy (temperature) terms, which used upwind schemes.

The turbulence was modelled with the k–ω Shear Stress Transport (SST) model (Menter, 1992). This model

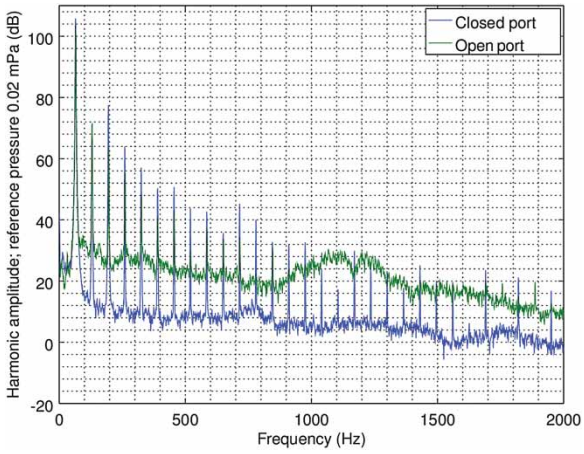

Figure 9. Comparison of the experimental results of the sound spectrum measured at 200 mm from the port with the bass-reflex ports open and closed when excited at 65 Hz.

works as a k–ω model near the walls and as a k–ϵ model in the far field (Casey & Wintergerste, 2000). As the vortices are created near the walls, a higher accuracy was required in those points and k–ω fulfils this constraint (Wilcox, 1993). According to Meslem, Bode, Croitoru, and Nastase (2014), the k–ω SST turbulence model works better than the k–ϵ and Reynolds Stress Models (RSM) in the near jet fluid flow.

The simulations have been carried out with a 64 AMD Opteron cores cluster, with 64 GB of memory. Two seconds were simulated for all cases, and each of them took about 130 hours with 3 processors. Only the steady-state, usually after around 30 cycles, was considered for the results. The cases simulated are with the original geometry excited with sinusoidal movement at different frequencies (40, 50, 65, 80 and 100 Hz) and with port geometry modifications (its radius, its length and its port end) at 65 Hz because this is the closest frequency to the Helmholtz frequency that could be reached experimentally. The internal performance of the enclosure with a closed port was also simulated.

3. Results

3.1. Experimental results

Both in experimental and numerical results, the frequency spectra were obtained with a Hanning window. From the comparison of the experimental results of the sound spectrum outside the port with the bass-reflex ports open and closed shown in Figure 9, it seems clear that the characteristic peak of noise in the bandwidth mentioned before is caused by the bass reflex. Moreover, there is no evidence of structural vibration in this frequency range of the port-induced noise (Figure 10), and it is reasonable to think that the blowing noise is caused by an aerodynamic effect of the shed vortices.

In order to verify that this behaviour is related to vortex shedding near the Helmholtz frequency, experiments for other frequencies were performed. Figure 11 shows the results for 315 Hz at a distance of 200 mm, and no

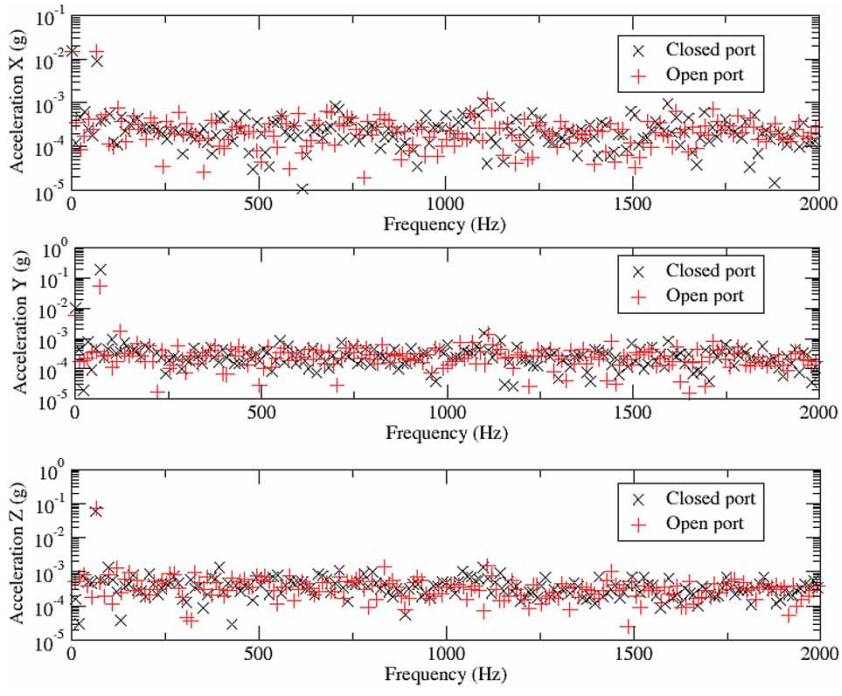

Figure 10. Comparison of the experimental results of the vibration spectrum of the cabinet with the bass-reflex ports open and closed when excited at 65 Hz. The three accelerations are simultaneously captured with the three-axis sensors shown in Figure 4.

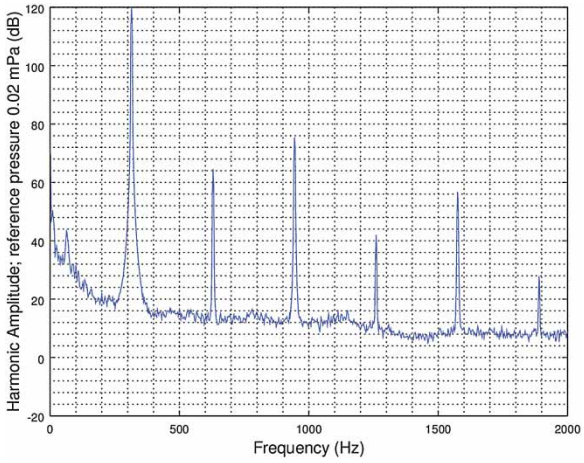

Figure 11. Experimental results of sound spectrum when excited at 315 Hz at 200 mm from the bass-reflex port.

evidence of noise in the 1000–1500 Hz range could be found.

With respect to the flow visualisation experiments, unfortunately the maximum frequency of the laser (3000 Hz) was insufficient to perform a proper PIV measurement, since the particle displacements were too large to get interrogation areas small enough for an adequate velocity field resolution. Nevertheless, with a particle tracking procedure estimation, considering the time delay and the spatial scale, the maximum velocity of the flow could be estimated as around 4 m/s, which roughly agrees in order of magnitude with reported results for similar experiments with PIV in other articles on this topic (Rossi et al., 2008), and a qualitative analysis could be done identifying the vortex structures in the flow. In Figure 12, the vortex image obtained with Ondine oil smoke is shown, along with its superimposition with numerical velocity, as depicted in Figure 13(c) after cropping and mirroring. Although no quantitative values of velocities are obtained, the vortex size and structure satisfactorily fit with the numerical computation.

3.2. Numerical results

In order to check the mesh suitability, a coarser mesh was tested. The surface averaged velocity in the bass-reflex port was calculated for two meshes: a fine mesh with almost 67,000 cells and a coarser mesh with near 43,000 cells. The results are presented in Figure 14. The time averaged velocity module for a period is 18.3 m/s for the fine mesh and 19.3 m/s for the coarse mesh, 5% larger. It is thus considered that the fine mesh suits the present simulation requirements, provided furthermore that it allows a better resolution of vortex shedding in the bass-reflex port.

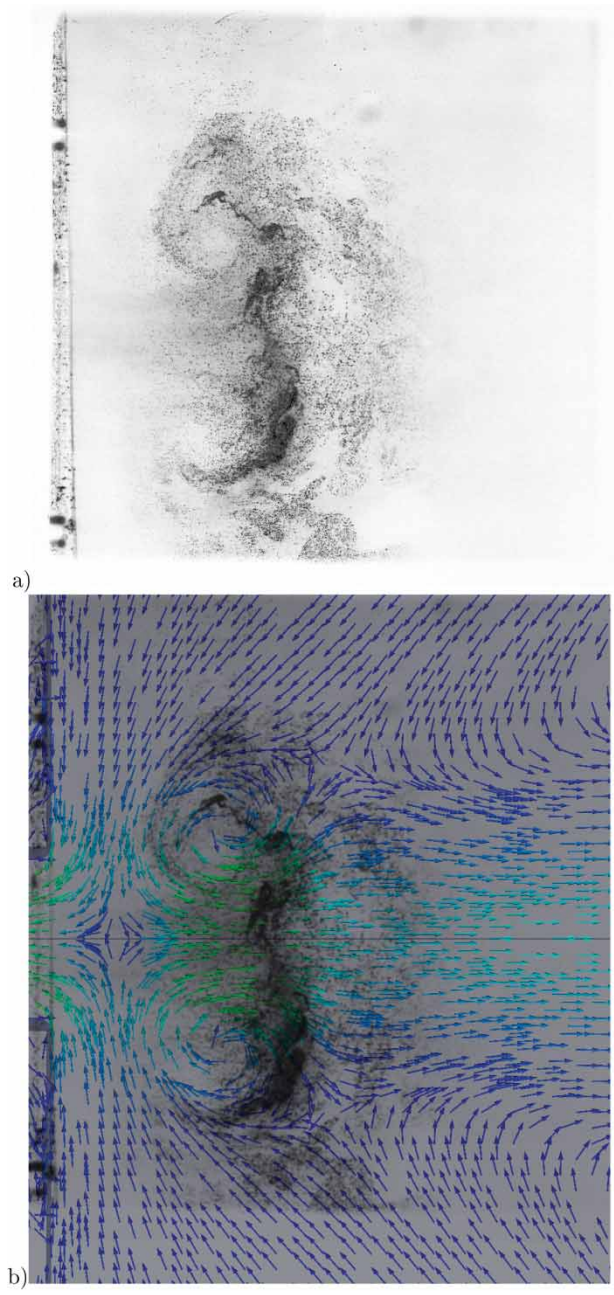

Figure 12. (a) Vortex structure in the port end captured with a flow visualisation experiment using Ondine oil smoke. (b) Same image superimposed with numerical velocity field results at 0.004 s taken from Figure 13(c).

The numerically produced sound was acquired outside the port. Figure 15 presents this pressure–time history, with a 7th-order Butterworth filter for low frequencies, for the case of a 65 Hz excitation signal, for 7 periods.

The pressure–frequency spectrum presents a characteristic pattern for all the different excitation frequencies used: an increase of sound pressure level in the bandwidth between 1000 and 1500 Hz that could be the origin of the noise produced by the vortices (see Figure 16). The

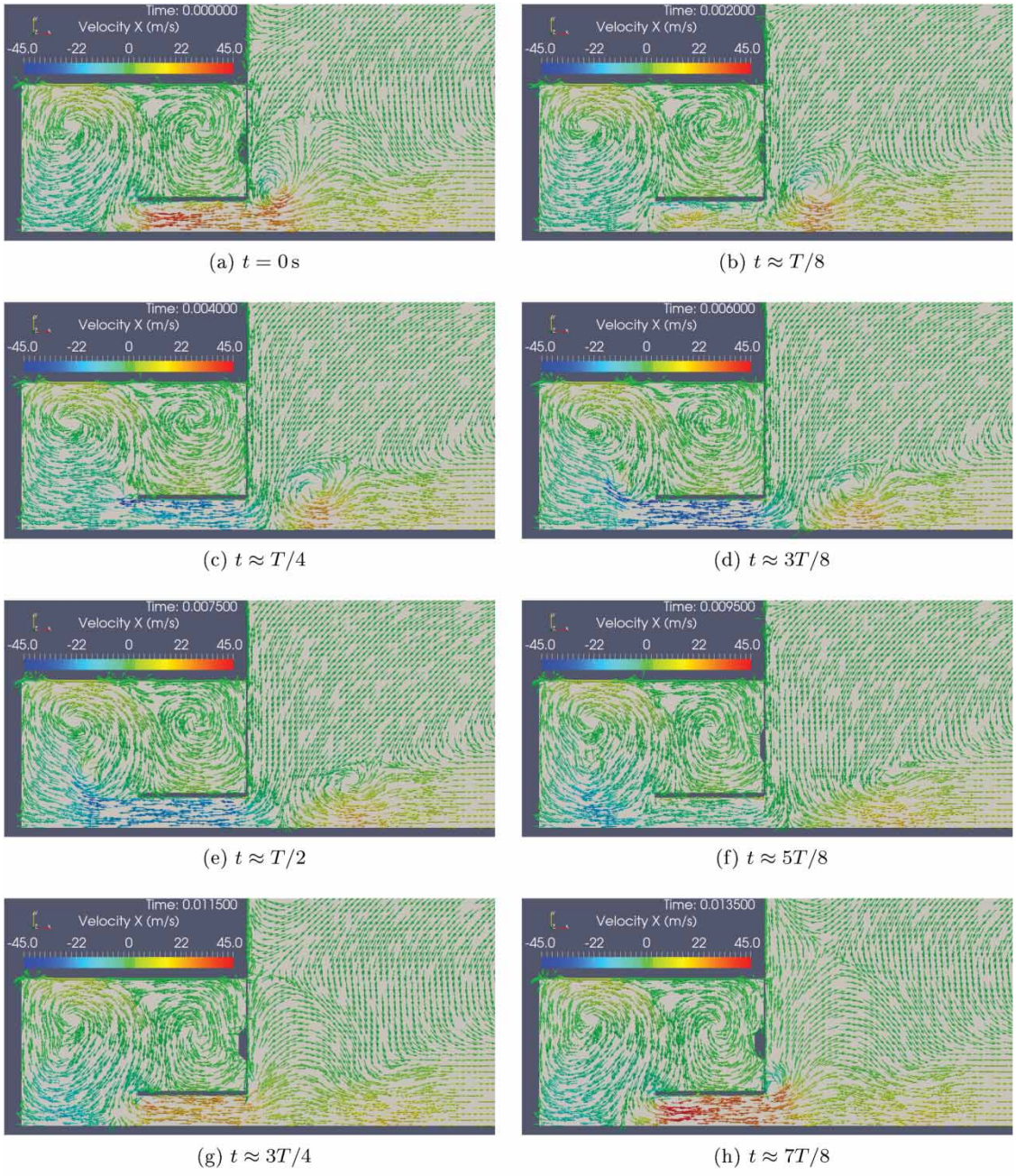

Figure 13. Velocity field at different instants for a 65 Hz excitation.

noise level increase can be more easily appreciated if the overall value is plotted against the frequency. In Figure 17 the mean noise level is plotted against excitation frequency for the 1000–1500 Hz frequency bandwidth and the overall (500–3000 Hz) frequency bandwidth. The mean noise increase is clear for the 1000–1500 Hz frequency bandwidth, where the noise level rises from 7 to nearly 20 dB.

In order to see the vortices, the invariant of the velocity gradient Q was calculated (Equation 8). This invariant takes positive values inside a vortex, where the enstrophy dominates, and negative values outside, where the strain product dominates (Bie, Hao, An, & Xu, 2016; da Silva & Pereira, 2008). The evolution of this field during one period of the 65 Hz simulation can be found in Figure 18.

$$Q = \sum_{i=1}^{3}\sum_{j=1}^{3} -\frac{1}{2}A_{ij}\cdot A_{ji} \quad \text{with } A_{ij} = \frac{\partial u_i}{\partial x_j}. \tag{8}$$

Pressure fields are depicted for the same times in Figure 19. Relative suction cores are visible in vortex centres and in the separation flow region at port ends.

The velocity fields for the same times are also shown in Figure 13 and the velocity field for the 3D simulation

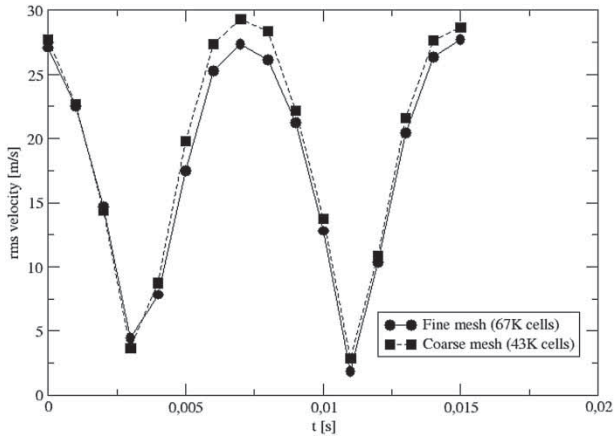

Figure 14. Root mean square of velocity in bass-reflex port in a period, for the fine mesh and the coarse mesh.

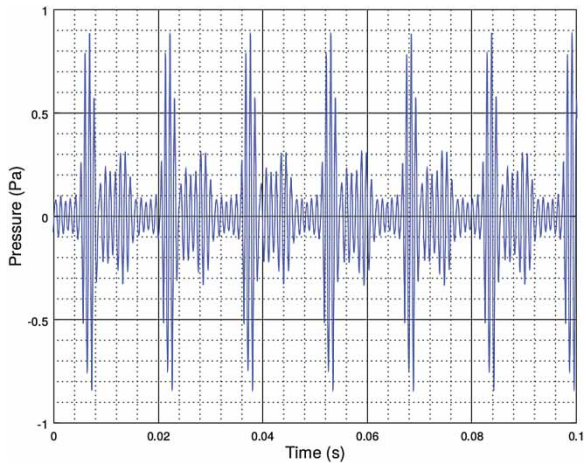

Figure 15. Time history of pressure measured in the probe at 0.2 m from the bass-reflex port exit. A 7th-order Butterworth filter was applied in order to filter low frequencies.

for $t \approx 7T/8$ is presented in Figure 5. In order to check the velocity values obtained numerically, a mass balance based estimation can be done. Considering the deforming volume in the loudspeaker enclosure and the exhaust velocity in the bass-reflex port, the mass balance is given by

$$\frac{\mathrm{d}}{\mathrm{d}t}\int_V \rho \,\mathrm{d}V + \int_{S_0} \rho u_n \,\mathrm{d}S = 0.$$

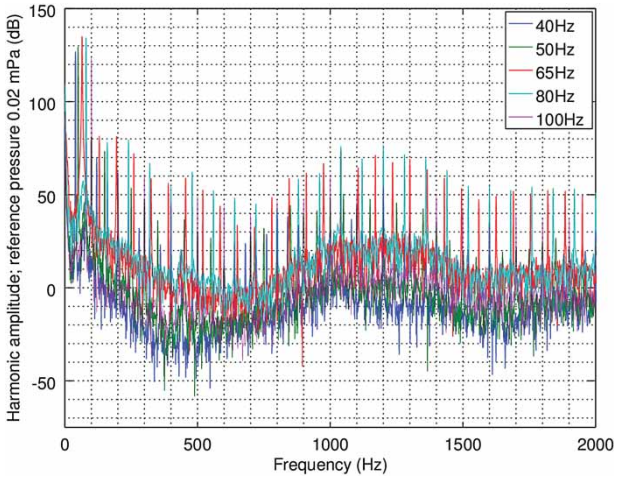

Figure 16. Numerical results of the sound spectrum at 20 cm outside the port for different excitation frequencies.

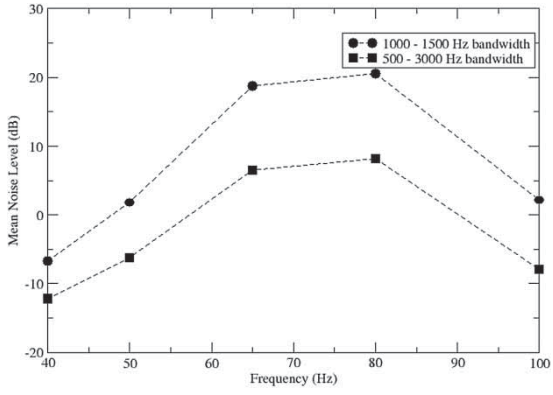

Figure 17. Mean noise level for the 1000–1500 Hz frequency bandwidth and the overall 500–3000 Hz frequency bandwidth. The noise level increase is noticeable in the 1000–1500 Hz frequency bandwidth in comparison with the overall mean level.

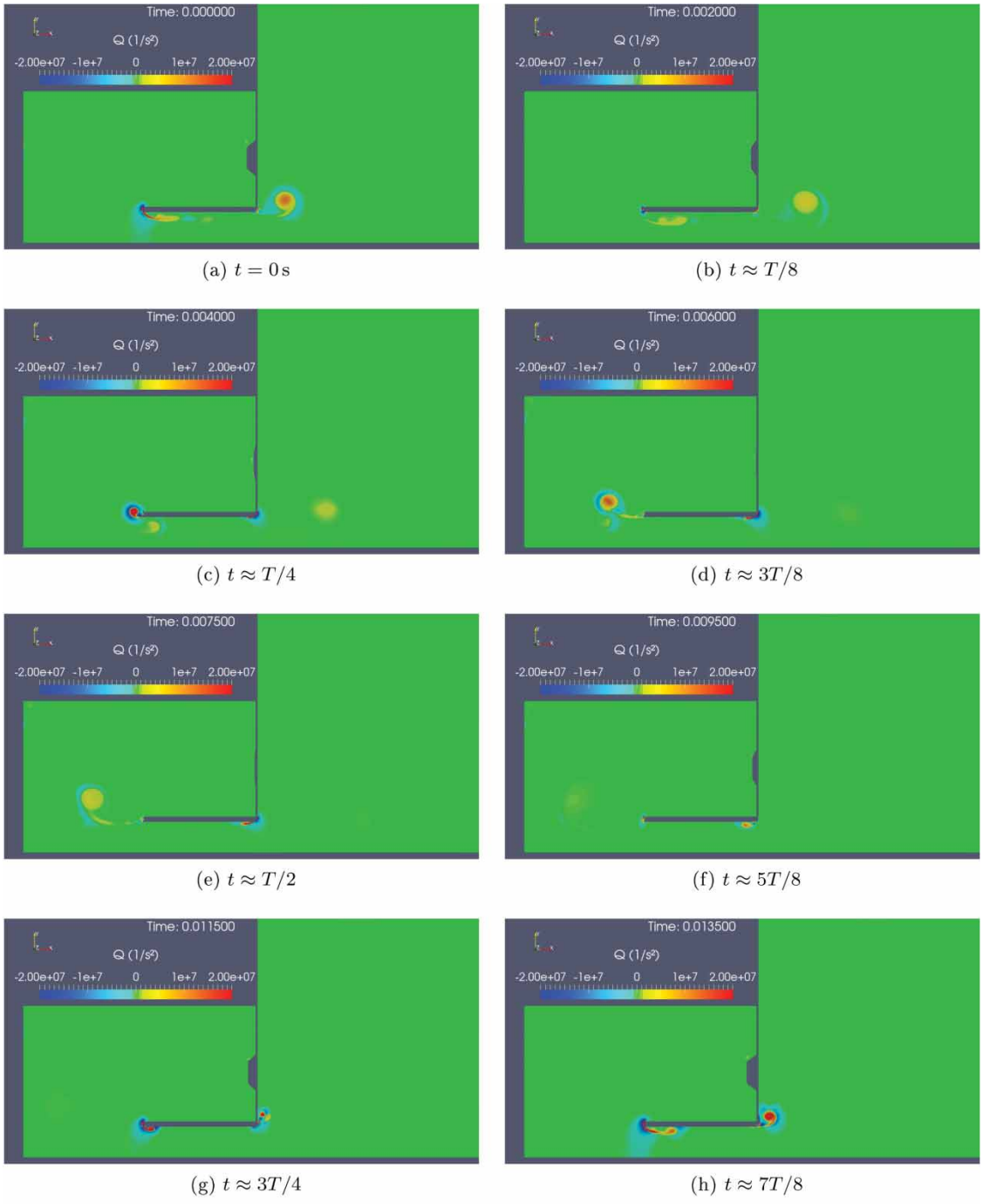

(a) $t = 0\,\mathrm{s}$ (b) $t \approx T/8$

(c) $t \approx T/4$ (d) $t \approx 3T/8$

(e) $t \approx T/2$ (f) $t \approx 5T/8$

(g) $t \approx 3T/4$ (h) $t \approx 7T/8$

Figure 18. *Q* field at different instant for a 65 Hz excitation.

Averaging in half a cycle, between the minimum volume and the maximum volume, this can be estimated as

$$\frac{\Delta}{\Delta t}(\rho V) + \bar{\rho}\bar{u}S_0 \approx \frac{(\rho V)_{\max} - (\rho V)_{\min}}{\Delta t} + \bar{\rho}\bar{u}S_0 = 0,$$

which yields an estimation of the exhaust mean velocity in the reflex port of

$$\bar{u} \approx \frac{(\rho V)_{\min} - (\rho V)_{\max}}{\Delta t \bar{\rho} S_0}.$$

A rough estimation of the density ranges from computational results of between 1.16 and 1.20 kg/m^3, a time interval of $\Delta t = 1/2f$, volumes of $V_{\max} = V/2 = 15.25 \times 10^{-3}$ m^3, $V_{\min} = V_{\max} - 2X_{\max}\pi(D^2/4)$, and a port surface of $S_0 = \pi R^2$ give the exhaust mean velocity as $\bar{u} \approx 17$ m/s.

In order to reinforce the argument that this increase of Sound Pressure Level (SPL) is produced by the bass-reflex port, a numerical simulation with the port closed

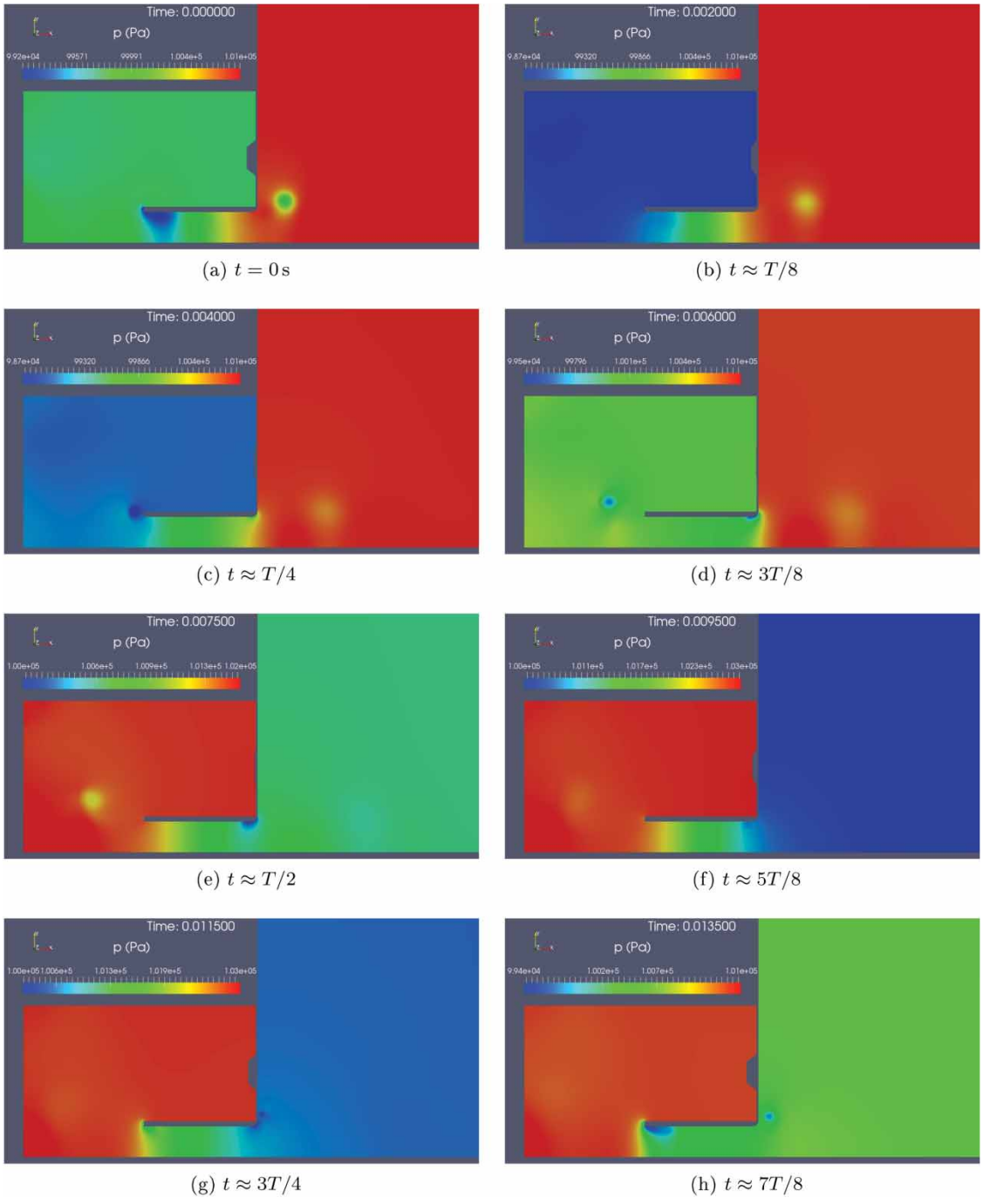

(a) $t = 0\,\mathrm{s}$ (b) $t \approx T/8$

(c) $t \approx T/4$ (d) $t \approx 3T/8$

(e) $t \approx T/2$ (f) $t \approx 5T/8$

(g) $t \approx 3T/4$ (h) $t \approx 7T/8$

Figure 19. Pressure field at different instants for a 65 Hz excitation.

was performed. For this case, several probes have been placed inside the enclosure, all over the axis. Two different behaviours have been found before and after the port. The numerical results presented in Figure 20 are the fast Fourier transform before entering the port, in the port end and inside the port in a closed port scenario. A peak at 790 Hz can be noted for the probes inside and outside the port, but not at the port end, which is due to the resonance between the walls in the axial direction. There is another peak at 680 Hz which has a bigger amplitude inside the port, but it gets attenuated in the box (outside the port). Nevertheless, the amplitude is negligible.

Geometric changes were applied trying to improve the device response and reduce the blowing sound. Specifically, changes in the radius and the length of the port were tested and the results are shown in Figures 21 and 22. By increasing the radius of the port, the noise level seemed to be reduced. However, this is not a real solution taking into account that, with this geometric change, the resonance frequency grows and becomes greater than 65 Hz.

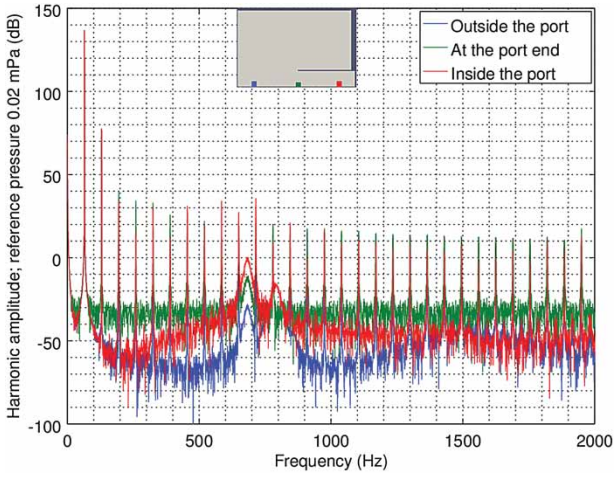

Figure 20. Numerical results for the sound spectrum in different probes placed over the axis considering the bass-reflex port closed for a 65 Hz excitation.

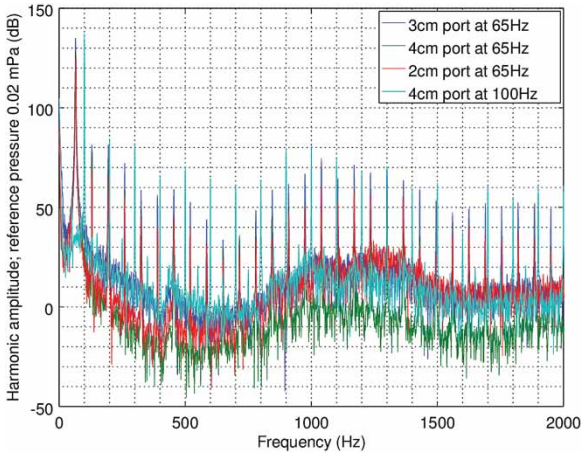

Figure 21. Effect of the port radius on the sound spectrum. Numerical results monitored at 20 cm from the port for different port radii and excitation frequencies.

In order to see the real effect, the results for an excitation frequency of 100 Hz (greater than the resonance frequency) is presented and no real improvement can be demonstrated.

Along the same lines, by changing the length of the port no clear improvement in noise intensity reduction can be found (see Figure 22).

4. Discussion

The sound radiated through the bass-reflex port was measured outside the enclosure. In the experimental case, the microphone was placed at 200 mm from the port on its axis, and for the numerical test the pressure probe was placed in the same location. Both approaches have been tested with four different frequencies: 40, 50, 65 and 80 Hz and with three different amplitudes: +22, +26

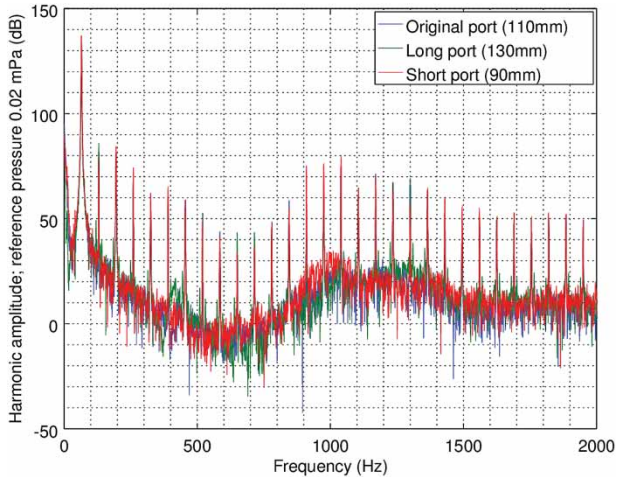

Figure 22. Effect of the port length on the sound spectrum when excited at 65 Hz. Numerical results computed at 20 cm from the port for different lengths.

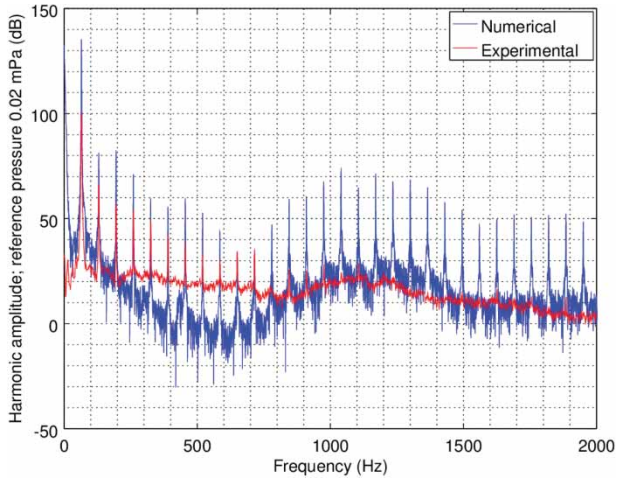

Figure 23. Comparison of the numerical and experimental sound spectrum results for an excitation frequency of 65 Hz.

and +30 *dBV*. The lowest of these was used to compare with the numerical results because of the higher accuracy of loudspeakers at low power. The comparison of numerical and experimental frequency spectra for a 65 Hz excitation signal can be seen in Figure 23. The numerical simulation properly reproduces the noise level in the frequency range of interest in the present work, between 1000 and 1500 Hz. Note the disagreement in the noise amplitude between numerical and experimental results in the range between 200 and 800 Hz. This cannot be attributed to the background noise level in the recording room, since it is not noted with the closed ports (Figure 9). Nevertheless, it could be an effect of the reduced absorption efficiency of walls in the anechoic chamber. It is worth remembering that the present model

reproduces only the acoustic signal produced by the bass-reflex port. Mechanical vibration (which can be stronger with an open port), 3D flow effects in the loudspeaker enclosure, and even the direct loudspeaker drive signal, are not considered in the numerical model. Any of these phenomena could be responsible for the disagreement in the 200–800 Hz bandwidth.

Likewise, the SPL for the harmonics is overestimated in the numerical simulations. In the first harmonic, the measured SPL is 100 dB, whereas for the numerical simulation it is around 135 dB. This behaviour has been reported previously in the technical literature (Dykas, Rulik, & Wróblewski, 2012; Dykas, Wróblewski, Rulik, & Chmielniak, 2010; Peng, 2005). This could be due to the closeness of the far field wave transmissive boundary condition in the outlet which, as noted above, is not able to transmit the pressure wave completely, and a small portion is reflected. In order to reduce the effect of this boundary condition, Bie et al. (2016) introduced a damp truncation region, which implies an additional source term in the numerical equations.

The results confirm that the numerical approach together with the axisymmetric hypothesis is a good approximation for a range of noise level increase between 1000 and 1500 Hz. In addition, the characteristic acoustic signal pattern is confirmed experimentally and numerically as evidence of the noise generated by the vortices. This model can lend valuable support to the design of circular bass-reflex ports in order to reduce the noise level produced by vortex shedding.

5. Conclusions

A cost-effective solution based on 2D axisymmetric geometry for the simulation of bass-reflex ports in loudspeaker enclosures is presented. It can be useful for the design and analysis of bass-reflex performance and blowing noise reduction. The origin of the noise generated by a bass-reflex port was detected. When it was excited at frequencies close to the Helmholtz frequency, notable vortex shedding was produced. The noise was found in the bandwidth between 1000 and 1500 Hz. Two-dimensional axisymmetric transient simulations were performed in order to reproduce this vortex generated noise. The agreement between experimental and numerical results was excellent in the bandwidth of the noise increase. Also, velocity and second invariant of velocity results have been presented in order to visualise the numerically generated vortices properly.

From the results of the flow visualisation experiment, the velocity field with the PIV methodology could not be determined with the available instrumentation, but the overall velocity of the flow in the interest region downstream from the port outlet was estimated at around 4 m/s. Moreover, a qualitative analysis was done identifying the vortex structures in the flow. However, although this is a first rough estimation, it allows qualitative comparison with numerical results.

The experimental testing showed that structural vibration could be excluded as a source of the noise in question. It has also been seen both experimentally and numerically that the noise disappears when the ports are closed. Therefore it can be concluded that the origin of the noise is aeroacoustical. A proper aeroacoustical simulation should be performed to analyse this phenomenon. A 3D simulation of the full geometry may be useful to check the obtained results, although it would require much more computer and time resources.

The influence of the geometry of the port was explored numerically. Changes in the radius and length do not show any significant difference in the performance of the port, especially in the noise range. By increasing the port diameter, the noise level decreases due to the variation in the exhaust velocity and, hence, the Strouhal number. Nevertheless, as noted above, a diameter increase also modifies the Helmholtz frequency and the port performance, and is not therefore a proper solution.

Acknowledgments

We would like to extend our appreciation to Dr Francisco Javier Freire, who has made suggestions and provided assistance in the accelerometer experiment, and to Dr Gustavo Raush for his valuable advice and interest in this study. In addition, we also would like to extent our gratitude to the technicians Justo Zoyo and Jaume Bonastre for their contribution in the experiments undertaken in this study.

Disclosure statement

No potential conflict of interest was reported by the authors.

ORCID

R. Castilla http://orcid.org/0000-0002-3848-2004
P.J. Gamez-Montero http://orcid.org/0000-0002-5168-3521
J. Romeu http://orcid.org/0000-0002-9075-6877
T. Pamies http://orcid.org/0000-0002-2994-9872

References

Backman, J. (1995). *The nonlinear behavior of reflex ports*. Presented at the Audio Engineering Society 98th Convention, 25–28 February 1995, Paris, France.

Backman, J. (2012). *Midrange resonant scattering in loudspeakers*. Audio Engineering Society 133rd Convention, 26–29 October 2012, San Francisco, CA.

Bie, H.-Y., Hao, Z.-R., An, W.-Z., & Xu, J. (2016). Simulations of cavity flow noise and turbulent jet noise using a hybrid method. *Advances in Mechanical Engineering*, *8*(2),

1–10. Retrieved from http://dx.doi.org/10.1177/1687814016632991

Casey, M., Wintergerste, T. (Eds.). 2000. *Best Practice Guidelines*. Brussels, Belgium: ERCOFTAC Special Interest Group on Quality and Trust in Industrial CFD.

da Silva, C. B., & Pereira, J. C. F. (2008). Invariants of the velocity-gradient, rateof-strain, and rate-of-rotation tensors across the turbulent/nonturbulent interface in jets. *Physics of Fluids*, *20*(5), Article ID 055101. Retrieved from http://dx.doi.org/10.1063/1.2912513

Dykas, S., Rulik, S., & Wrblewski, W. (2012). Numerical modelling of aerodynamic noise in compressible flows. *Open Journal of Fluid Dynamics*, *2*(03), 65–69.

Dykas, S., Wróblewski, W., Rulik, S., & Chmielniak, T. (2010). Numerical method for modeling of acoustic waves propagation. *Archives of Acoustics*, *35*(1), 35–48.

Greenshields, C. J. (2015). *OpenFOAM – The Open Source CFD Toolbox*. Programmer's Guide (version 2.4.0) [Computer software manual]. Reading, UK: The Open-FOAM Foundation.

Menter, F. (1992). *Improved two-equation k–! turbulence models for aerodynamic flows (Technical Memorandum 103975)*. Moffett Field, CA: NASA. Retrieved from https://ntrs.nasa.gov/archive/nasa/casi.ntrs.nasa.gov/19930013620.pdf

Meslem, A., Bode, F., Croitoru, C., & Nastase, I. (2014). Comparison of turbulence models in simulating jet flow from a cross-shaped orifice. *European Journal of Mechanics - B/Fluids*, *44*, 100–120. Retrieved from http://dx.doi.org/10.1016/j.euromechflu.2013.11.006

Middelberg, J., Barber, T., Leong, S., Byrne, K., & Leonardi, E. (2004). Computational fluid dynamics analysis of the acoustic performance of various simple expansion chamber mufflers. In *Proceedings of the 2004 Annual Conference of the AustralianAcoustical Society*, 3–5 November 2004, Gold Coast, Australia (pp. 123–127).

Peng, S.-H. (2005). *Unsteady RANS Simulation of Turbulent Cavity Flow: Summary of 2D Baseline Computations*. Stockholm: Totalförsvarets forskningsinstitut (FOI).

Poinsot, T. J., & Lelef, S. (1992). Boundary conditions for direct simulations of compressible viscous flows. *Journal of Computational Physics*, *101*(1), 104–129.

Rapoport, Z., & Devantier, A. (2004). *Analysis and modeling of the bi-directional fluid flow in loudspeaker ports*. Presented at the Audio Engineering Society 117th Convention, 28–31 October 2004, San Francisco, CA.

Roozen, N. B., Bockholts, M., van Eck, P., & Hirschberg, A. (1998a). Vortex sound in bass-reflex ports of loudspeakers. *Part II. A method to estimate the point of separation. The Journal of the Acoustical Society of America*, *104*(4), 1919–1924.

Roozen, N. B., Bockholts, M., van Eck, P., & Hirschberg, A. (1998b). Vortex sound in bass-reflex ports of loudspeakers. *Part I. Observation of response to harmonic excitation and remedial measures. The Journal of the Acoustical Society of America*, *104*(4), 1914–1918.

Roozen, N. B., Vael, J. E. M., & Nieuwendijk, J. A. (1998). *Reduction of bass-reflex port nonlinearities by optimizing the port geometry*. Presented at the Audio Engineering Society 104th Convention, 16–19 May 1998, Amsterdam, The Netherlands.

Rossi, M., Esposito, E., & Tomasini, E. P. (2008). PIV application to fluid dynamics of bass reflex ports. In A. Schroeder & C. E. Willert (Eds.), *Particle Image Velocimetry: New Developments and Recent Applications* (pp. 259–270). Berlin: Springer.

Salvatti, A., Devantier, A., & Button, D. J. (2002). Maximizing performance from loudspeaker ports. *Journal of the Audio Engineering Society*, *50*(12), 19–45.

Schmalz, J., & Kowalczyk, W. (2015). Implementation of acoustic analogies in Open-FOAM for computation of sound fields. *Open Journal of Acoustics*, *5*(2), 29–44.

Torregrosa, A. J., Fajardo, P., Gil, A., & Navarro, R. (2012). Development of nonreflecting boundary condition for application in 3D computational fluid dynamics codes. *Engineering Applications of Computational Fluid Mechanics*, *6*(3), 447–460. Retrieved from http://dx.doi.org/10.1080/19942060.2012.11015434

Vanderkooy, J. (1998). *Nonlinearities in loudspeaker ports*. Presented at the Audio Engineering Society 104th Convention, 16–19 May 1998, Amsterdam, The Netherlands.

Weller, H., Tabor, G., Jasak, H., & Fureby, C. (1998). A tensorial approach to computational continuum mechanics using object-oriented techniques. *Computers in Physics*, *12*(6), 620–631.

Wilcox, D. (1993). *Turbulence Modeling for CFD*. La Cañada Flintridge, CA: DCW Industries.